Journal of Solid State Chemistry **161,** 355–364 (2001)
doi:10.1006/jssc.2001.9343, available online at http://www.idealibrary.com on IDEAL®

Structural and Superconducting Properties of $Hg_{0.75}Re_{0.25}Ba_{2-x}Sr_xCa_2Cu_3O_{8+\delta}$ Superconductors Grown by Sol–Gel and Sealed Quartz Tube Synthesis

A. Sin,*,[1] F. Alsina,† N. Mestres,† A. Sulpice,‡ P. Odier,* and M. Núñez-Regueiro‡

*Laboratoire de Cristallographie-CNRS, 25 Av. des Martyrs, B.P. 166, F-38042 Grenoble Cedex 09, France; †Institut de Ciència de Materials de Barcelona (CSIC), Campus de la UAB, Bellaterra, E-08193, Barcelona, Spain; and ‡Centre de Recherche sur les Très Basses Températures-CNRS, 25 Av. des Martyrs, B.P. 166, F-38042 Grenoble Cedex 09, France

Received May 14, 2001; accepted August 2, 2001

The structural and superconducting properties of $Hg_{0.75}Re_{0.25}Ba_{2-x}Sr_xCa_2Cu_3O_{8+\delta}$ ($x = 0.0$, 0.2, 0.4, 0.6, 0.8, 1.0) grown by sol–gel and sealed quartz tube synthesis were investigated through XRD, EDX, and micro-Raman analysis. They show that the efficiency of *c*-axis reduction caused by the Sr substitution depends on the environment in the (Hg, M)–O layer. The rhenium doping produces a more rigid block that limits the Sr substitution in the Ba site more than other reported doping cations, such as lead. Superconducting properties measurements show that the irreversibility line (IL) values decrease with increasing Sr substitution. Moreover, the IL line measurements also show that the vortex lines have a 3D behavior for all the samples with *n* values in the range 2.1–1.9. Finally, resistivity measurements under high pressure indicate an overdoped regime for these samples. © 2001 Academic Press

1. INTRODUCTION

The highest T_c until now (134 K) has been achieved in $HgBa_2Ca_2Cu_3O_{8+\delta}$ superconductors (1). As a general result, application of pressure on these superconducting cuprates increases the T_c for underdoped and optimally doped compounds. For example, T_c of $HgBa_2Ca_2Cu_3O_{8+\delta}$ increases to 164 K at 30 GPa (2, 3). It is generally considered that application of pressure promotes transfer of charge from the reservoir block to the superconducting block (4). In underdoped superconductors the pressure increases T_c by doping, while a decrease of T_c is observed in overdoped cuprates.

On the other hand, application of chemical pressure is a very attractive way to reproduce naturally this mechanical pressure effect on superconductivity. One possible way involves substituting Ba by smaller cations such as Sr. This type of substitution has been performed in several works trying to achieve this goal (5–7). However, all the experiments produced a reduction of T_c. Nevertheless, the strontium substitution provides other interesting advantages from the point of view of the applications. This substitution produces a contraction of the blocking block, i.e., $\{(Hg,M)O_{(4)}–(Ba,Sr)O_{(3)}\}$, providing a stronger coupling between the conducting blocks, i.e., $\{CuO_2–Ca–CuO_2–Ca–CuO_2\}$, and could decrease the electronic anisotropy (γ) which is an important parameter for increasing the irreversibility fields (8). Nevertheless, the occupation of oxygen in the $HgO_{(4)\delta}$ plane becomes very unfavorable as the unit cell contracts with increasing strontium substitution in the nondoped systems (9). This effectively reduces the average coordination number of the alkaline earth ion, producing a nonsatisfied nine-fold capped square antiprismatic site (see Fig. 1) (10). Therefore, doping by a high-valence metal in the mercury site provides the oxygen of the $HgO_{(4)\delta}$ plane necessary for the superconducting structure stabilization. Re substitution in the mercury site produces an additional contraction of the blocking block. Moreover, it has been proved that Re doping in Sr-free samples stabilizes their chemical structure and handling procedure in the sealed quartz tube synthesis (11). Additionally, it improves their superconducting properties such as the irreversibility field (12), making them suitable for practical applications.

In this work, we report a comparative study of the structural and superconducting properties of $Hg_{0.75}Re_{0.25}Ba_{2-x}Sr_xCa_2Cu_3O_{8+\delta}$ ($x = 0.0$, 0.2, 0.6, 1.0). XRD, EDX, and micro-Raman analyses are performed to probe the structural effects induced by Sr substitution. These analyses show that the efficiency of *c*-axis reduction caused by Sr substitution depends on the environment in the $(Hg,M)–O_{(4)}$ layer. In a rhenium-doped system the solubility of the Sr is lower than other less acidic cations, such as

[1]To whom correspondence should be addressed. Present address: Pirelli Labs S.p.A., Viale Sarca 222, 20126 Milano, Italy. Fax: + 39 02 6442 9431. E-mail: agustisin@hotmail.com, agusti.sin@ pirelli.com.

0022-4596/01 $35.00

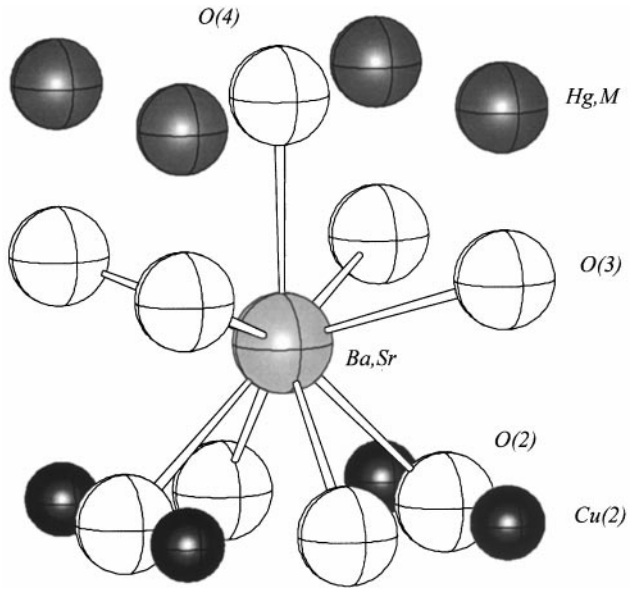

FIG. 1. Detail of the {(Hg,M)O–(Ba,Sr)O} block. The bonding lines highlight the nine-fold oxygen coordination of the (Ba,Sr) site.

lead. Superconducting properties measurements such as dc susceptibility, irreversibility line (IL), and resistivity under high pressure are also performed. We have found that T_c decreases when the strontium substitution is increased. Also, the higher IL values correspond to Sr-free samples and the values decrease with increasing Sr substitution, even for the samples in the overdoped regime as checked by resistivity under high-pressure measurements. Moreover, the IL shows that the vortex lines have a 3D behavior for all the samples with n values between 2.1–1.9.

2. EXPERIMENTAL

The synthesis of "$Re_{0.25}Ba_{2-x}Sr_xCa_2Cu_3O_x$" nanopowders is carried out following the same procedure as reported in Refs. (9, 13). It begins by dissolving separately $CaCO_3$ (Diopma 99.95%), $SrCO_3$ (Aldrich 99%), CuO (Diopma 99.99%), and Re (Aldrich 99.99%) in nitric acid, and $BaCO_3$ (Diopma 99.9%) in acetic acid. The solutions are mixed afterward in the stoichiometric ratio. The Cu^{2+} and Re^{6+} solution is complexed with acid–EDTA: $(H_4Y) = [CH_2N(CH_2COOH)_2]_2$ (Prolabo 98%) in the ratio 1:1 and the pH adjusted to ≈ 3 with ammoniac addition to obtain H_2Y^{2-}, a species that best complexes with the cation. Finally, all the solutions are mixed in the presence of water to reach a total volume of approximately 200 ml for obtaining 25 g of precursor phase. To this solution is added 16 g of acrylamide monomers (Aldrich 99 + %), i.e., $H_2C=CHCONH_2$; 1.6 of N,N'-methylenebisacrylamide (Aldrich 99%), i.e., $(H_2C=CHCONH)_2CH_2$, and a few milligrams of a reticulating agent α,α'-azoisobutyronitrile (Fluka 98 + %), i.e., $C_8H_{12}N_4$, to perform the polymerization which is easily achieved by heating to 80°C. This forms monolithic gels that are stable with time.

The gel is then dried for a few minutes in a microwave oven. During this process, the dehydration occurs firstly and is then followed by the ignition of part of the organic phases, which should be controlled to avoid aggressive exothermic reactions. The procedure results in a porous foam material. The xerogels obtained are then homogenized in a ceramic mortar and calcined at 870°C for 5 h in a muffled furnace with circulation of N_2 gas.

The synthesis of the superconducting ceramic ($Hg_{0.82}Re_{0.18}Ba_{2-x}Sr_xCa_2Cu_3O_{8+\delta}$) is performed by the sealed quartz tube method. The precursor obtained is then mixed with HgO (99%, Aldrich) in nominal stoichiometric quantity. The resulting powder is pelletized, wrapped in a gold foil with a 5% of excess of Hg(1) (10), and inserted in a quartz tube that is closed under vacuum. The filling factor referring to the ratio between the sample mass and the capsule volume is ~ 1.0 g/cm^3. The thermal treatment starts with the introduction of the sample into a preheated furnace at 850°C to avoid the formation of $HgCaO_2$ (14). The holding time was 10 h at this maximum temperature. The furnace is then cooled at 120°C/h.

The XRD pattern was obtained by using Cu$K\alpha$ radiation in a Siemens D-5000 diffractometer. The EDX analysis was carried out by using a Jeol JSM-6300 system with Link ISIS 3.00 (Oxford) software. The ceramic samples analyzed were cleaved and polished without any lubricant. Micro-Raman measurements were performed at room temperature by using a Jobin Yvon T64000 triple spectrometer equipped with a charge-coupled device (CCD) detector and an Olympus metallurgical microscope. The excitation was provided by the 514.5-nm line generated by an Ar^+ laser. All Raman spectra were recorded in a back scattering geometry using the microprobe optics, which can focus the laser beam down to 1 μm (objective × 100) on a single crystallite. Rectangular crystallites (typically 3×15 μm^2) with the shortest edge corresponding to the c-axis, and with an optically clean specular surface, were chosen under the microscope on the surface of the polycrystalline sample. All spectra were collected in the $x(z, z)x$ polarization configuration (z along the c direction), in which only Raman modes of A_{1g} symmetry are allowed. The magnetization measurements are performed in a commercial SQUID instrument (Metronique Ingenierie). The electrical resistivity measurements were performed in a sintered diamond Bridgman anvil apparatus using a pyrophillite gasket and two steatite disks as the pressure medium. The Cu–Be device that locked the anvils can be cycled between 1.2 K and 300 K in a sealed dewar. Pressure was calibrated against the various phase transitions of Bi under pressure at room temperature and by superconducting Pb manometer at low temperature. The overall uncertainty in

the quasi-hydrostatic pressure is estimated to be $\pm 15\%$. The pressure spread across the sintered diamond anvils was previously determined on Pb manometers to be about 1.5–2 GPa, depending on the applied pressure. The temperature was determined by using a calibrated carbon glass thermometer with a maximum uncertainty (due mainly to temperature gradients across the Cu–Be clamp) of 0.5 K. Four-probe electrical resistivity measurements were made using a Keithley 2182 nanovoltmeter combined with a Keithley 220 current source.

3. RESULTS AND DISCUSSION

3.1. XRD and EDX Analysis

The X-ray diffraction patterns corresponding to the $Hg_{75}Re_{25}Ba_{2-x}Sr_xCa_2Cu_3O_y$ samples with different nominal Sr stoichiometries ($x = 0.0$, 0.2, 0.4, 0.6, 0.8, 1.0) are shown in Fig. 2. The quality of the samples seems to depend on the Sr concentration, although all the samples are prepared under the same conditions. The main impurities are $HgCaO_2$, unreacted precursor phases ($BaCuO_2$, $Ba_4Re_2CaO_{12}$, CuO, CaO), and other unidentified impurities. One observes that the $n = 3$ phase is dominant close to $x \approx 0.8$, and that higher x values imply an important increase of the percentage of impurities. Therefore, we can say that $x = 1.0$ is the solubility limit for obtaining (Hg,Re)-1223 as a main phase.

Nevertheless, it has been reported that a total substitution of the Ba for Sr with high quality is possible only under high-pressure synthesis (15–19). Total Sr substitution in the Re-doped (10) and Pb-doped (20) systems by the sealed quartz tube method has also been reported. However, the authors have remarked an important presence of impurities in the bulk ceramic. Nevertheless, good-quality samples with $x = 1.5$ have been obtained in the Pb-doped system. This fact seems to indicate that this doping allows a higher Sr substitution in the superconducting cell using the sealed-tube technique.

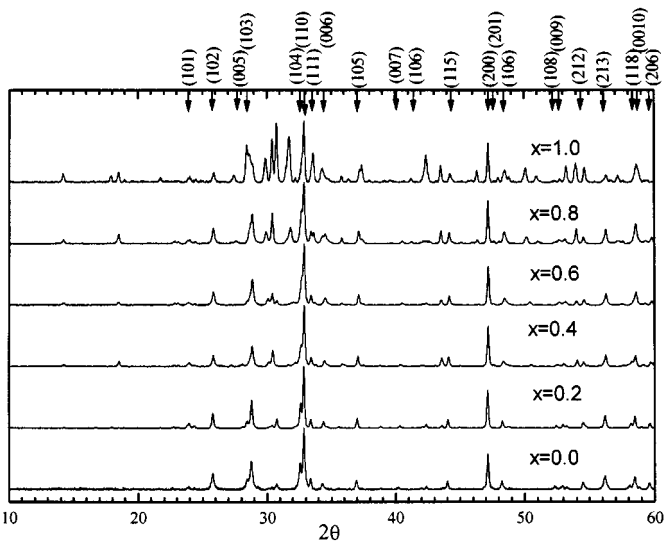

FIG. 2. XRD powder pattern of $Hg_{0.75}Re_{0.25}Ba_{2-x}Sr_xCa_2Cu_3O_y$ ($x = 0.0$, 0.2, 0.4, 0.6, 0.8, 1.0). Indexed peaks correspond to the (Hg,Re)-1(Ba,Sr)223 phase.

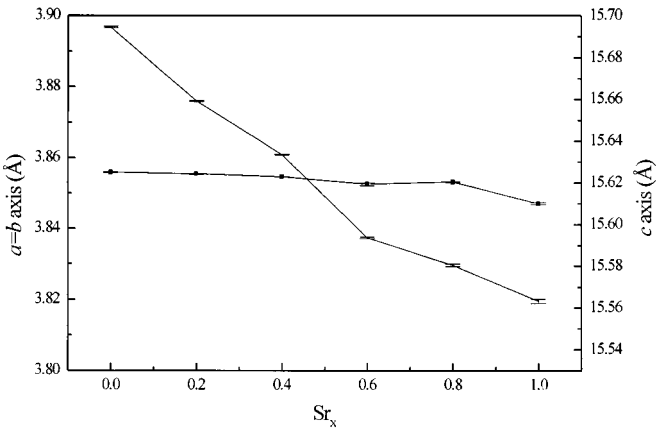

FIG. 3. Variation of the $a = b$ and c-axis parameters as a function of the nominal Sr substitution.

The crystallographic axes have been calculated from the X-ray diffraction patterns using a tetragonal cell ($P4/mmm$), and the values obtained are displayed in Fig. 3. We can observe a clear decrease of the c parameter with increasing nominal Sr content while the $a = b$ parameter suffers only a slight contraction. The c-axis undergoes a lower reduction above $x = 0.6$; this could be a sign of the difficult substitution of Ba by Sr above this value.

In the following, we analyze the reduction of the c-axis of the Hg-1223 cell due to Sr substitution by comparing the values of the c-axis for undoped Hg-1(Ba,Sr)223 (5, 21) and (Hg,M)-1(Ba,Sr)223 (where M = Re (this work) and Pb (Ref. 20)) for Sr substitution of $x = 0.0$ and $x = 1.0$. The c-axis values for the metal-doped systems corresponding to the Re-doped (this work) and the Pb-doped samples (20), with the same strontium substitution ($x = 1.0$), are $c = 15.563(1)$ Å and $c = 15.60$ Å (Ref. 20), respectively, and $c = 15.6945(3)$ Å and $c = 15.84$ Å (Ref. 20) for the Sr-free samples. In addition, it is interesting to compare these data with a reference sample of Hg-1223 Sr-free without doping with $c = 15.7782$ Å (Ref. 21) and $c = 15.540(6)$ Å (Ref. 5) for $x = 1.0$. We want to highlight that the synthesis of undoped phase with strontium substitution is possible only under the high-pressure technique (5). All these data are summarized in Table 1.

First, regarding the c-axis value of Sr-free samples (Table 1), it is observed that rhenium doping (15.6945(3) Å) provides a reduction of the c-axis with respect to the

TABLE 1
***c*-Axis Values in Angstroms of Different (Hg,M)-1(Ba,Sr)223 Samples**

	$x = 0.0$	$x = 1.0$	Δc
$HgBa_{2-x}Sr_xCa_2Cu_3O_{8+\delta}$[a]	15.7782[21]	15.540(6)[5]	0.23
$Hg_{0.7}Pb_{0.3}Ba_{2-x}Sr_xCa_2Cu_3O_{8+\delta}$[b]	15.84[20]	15.60[20]	0.24
$Hg_{0.75}Re_{0.25}Ba_{2-x}Sr_xCa_2Cu_3O_{8+\delta}$[b]	15.6945(3) (this work)	15.563(1) (this work)	0.13
$Hg_{0.78}Re_{0.22}Ba_{2-x}Sr_xCa_2Cu_3O_{8+\delta}$[a]	15.7036(3)[22]	15.4372(4)[c,15]	0.26

[a]High-pressure synthesis.
[b]Sealed quartz tube synthesis.
[c]Linear-extrapolated value.

undoped samples (15.7782 Å), while lead doping increases it (15.84 Å). Therefore, if we assume that the main contraction corresponds to the blocking block, i.e., $\{(Hg,M)O_{(4)}–(Ba,Sr)O_{(3)}\}$ (15, 22), in the same sense as when a high external pressure is applied (23), we can say that the rhenium doping contracts this region better for the Sr-free sample. To understand the *c*-axis reduction produced by the rhenium doping we can compare the ionic radii of the cations. The Re^{6+} and the Pb^{4+} have coordination numbers of six and two for Hg^{2+}, which correspond to 0.55, 0.75, and 0.69 Å, respectively. This fact can explain the higher contraction of the blocking block due to Re doping, compared with the nondoped system, and the expansion caused by Pb doping.

When strontium is substituted in a barium site, all samples reduce considerably their *c*-axis and fall close to the same value (15.540(6), 15.563(1), and 15.60 Å for undoped, Re-doped, and Pb-doped, respectively), producing a higher contraction than any made by metal doping in the mercury site.

In all the cases (lead, rhenium, or without doping), the variation of *c*-axis for a strontium substitution between $x = 0.0$ up to 1.0 corresponds to $\Delta c \approx 0.23–0.26$ (Table 1) (51, 15, 20). Nevertheless, in our samples we obtain a $\Delta c = 0.13$ that could be a sign of a lower Sr substitution with respect to the nominal composition. Therefore, it is possible that the nominal strontium substitution deviates from the real value. This could be attributed to the stress and rigidity introduced in the blocking block by the rhenium. It certainly hinders a further shortening of this interlayer distance, as Ba is replaced by Sr, making it difficult to stabilize this substitution. This fact will be discussed later in the micro-Raman analysis. However, only synthesis under high pressure can solve this problem and achieve a total Sr substitution in the rhenium samples (15). If we extrapolate their *c*-axis data (15) for $x = 1.0$ we obtain a $\Delta c = 0.23$, in the same order as for the undoped and Pb-doped systems. The rigidity and inflexibility caused by the rhenium in the blocking block can then affect negatively the strontium solubility in the barium site. As a consequence, the production of high-quality samples above $x = 1.0$ for the Re-doped samples using only the sealed quartz tube technique becomes a very difficult challenge.

An EDX analysis was performed to verify the strontium composition. The results shown in Fig. 4 confirm the Sr substitution in the (Hg,Re)-1223 cell. However, a little shift toward an excess from the ideal stoichiometry is observable. We relate this fact to the overlapping position of the Re and Sr lines that use the probe for this analysis. However, evolution of the Sr at a few percent value is clear, in agreement with the XRD data. Nevertheless, we assume that it could be a lack of strontium referred to the nominal composition.

We can then say that the efficiency of the *c*-axis reduction caused by Sr substitution depends on the environment in the $(Hg,M)–O_{(4)}$ layer when the sealed-tube synthesis is used.

3.2. *Micro-Raman Analysis*

Micro-Raman spectroscopy is known as a powerful tool to study lattice dynamics and charge redistribution effects in ceramic superconductor samples. We use this technique to study changes in the lattice dynamics due to Sr substitution into the Ba site in (Hg,Re)-1223 samples. As was described previously, strontium substitution in the barium site leads to a reduction of the crystal lattice. Therefore, an increase of the mode frequencies observed in the Raman spectrum is expected. Figure 5 displays the Raman spectra of the $Hg_{0.75}Re_{0.25}Ba_{2-x}Sr_xCa_2Cu_3O_{8+\delta}$ samples, for $x = 0.0$, 0.6, and 1.0. All spectra were collected in the $x(z, z)x$ polarization configuration (z along the *c* direction), in which

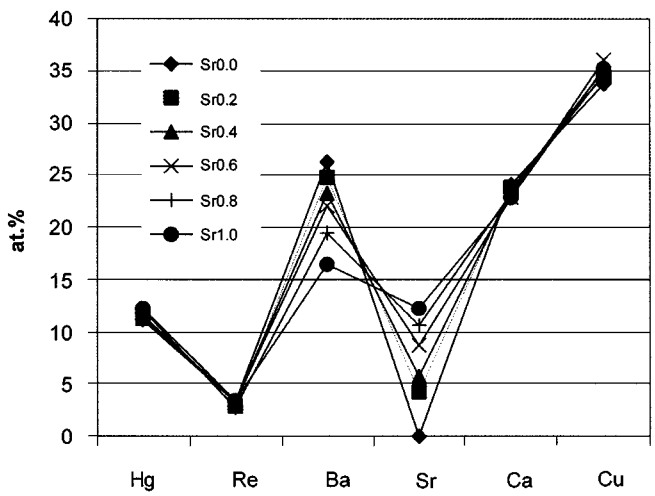

FIG. 4. Atomic percentage of $Hg_{0.75}Re_{0.25}Ba_{2-x}Sr_xCa_2Cu_3O_y$ ($x = 0.0$, 0.2, 0.4, 0.6, 0.8, 1.0) from EDX analysis.

only Raman modes of A_{1g} symmetry are allowed. The main peak intensities were obtained from the least-squares fits using Lorentzians. We obtain 573, 590, 639, 749, 780, 798, 807, and 862 cm^{-1} for the $x = 0.0$ sample. On the basis of previous mode assignment for Hg-1223 (24–27), the peak at 590 cm^{-1} can be readily assigned to the A_{1g} mode vibrations concerning the apical oxygen in the Hg–$O_{(3)}$–Cu bond. The peak at 570 cm^{-1} has been assigned to the A_{1g} mode of the same apical oxygen but modified by the presence of the oxygen placed in the Hg plane. In previous work (27), it has been shown that Re-doped samples show a Raman signal at high energy, 638 cm^{-1}. This signal increased in intensity with increasing nominal rhenium content. Therefore, this mode was assigned to the A_{1g} vibrations of the apical oxygen in the Re–$O_{(3)}$–Cu bond. The Hg-1223 structure with A_{1g} mode vibration of the apical oxygen ($O_{(3)}$) is schematized in Fig. 6. The Re–$O_{(3)}$ bond has to be stronger than the Hg–$O_{(3)}$ bond (6, 7); this could be explained by comparing the acid character between Re and Hg ions. The acid cation definition consists of a charge/radii ratio. The rhenium, in the superconducting cell, has a higher valence (+6) than Hg (+2), and the smaller radius of the Re^{6+} (0.55 Å) ion, compared to that of Hg^{2+} (0.69 Å), leads to a much higher acid character of the rhenium cation (10.90 and 2.89, respectively). High acid character of a cation means a high percentage of covalent bonding character with its coordinated atoms, increasing the structural rigidity. It is then reasonable to assume that the stretching motion of the

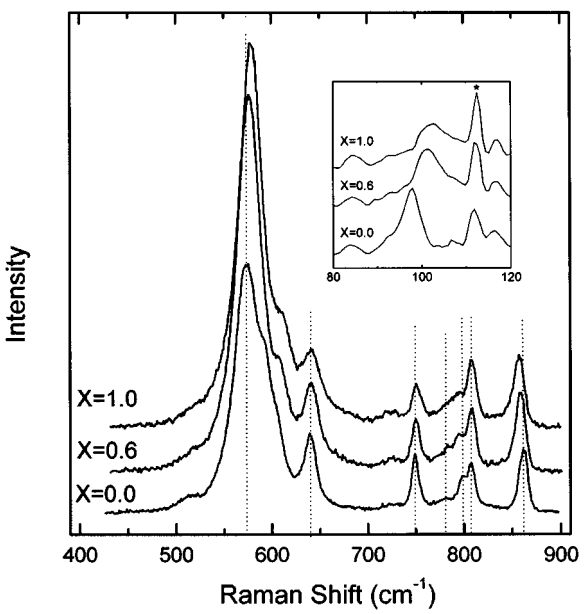

FIG. 5. Raman spectra of the $Hg_{0.75}Re_{0.25}Ba_{2-x}Sr_xCa_2Cu_3O_y$ samples with different Sr substitution taken in the $x(zz)x$ configuration. The inset shows the evolution of the low-frequency mode. The peak marked with an asterisk corresponds to a laser plasma line.

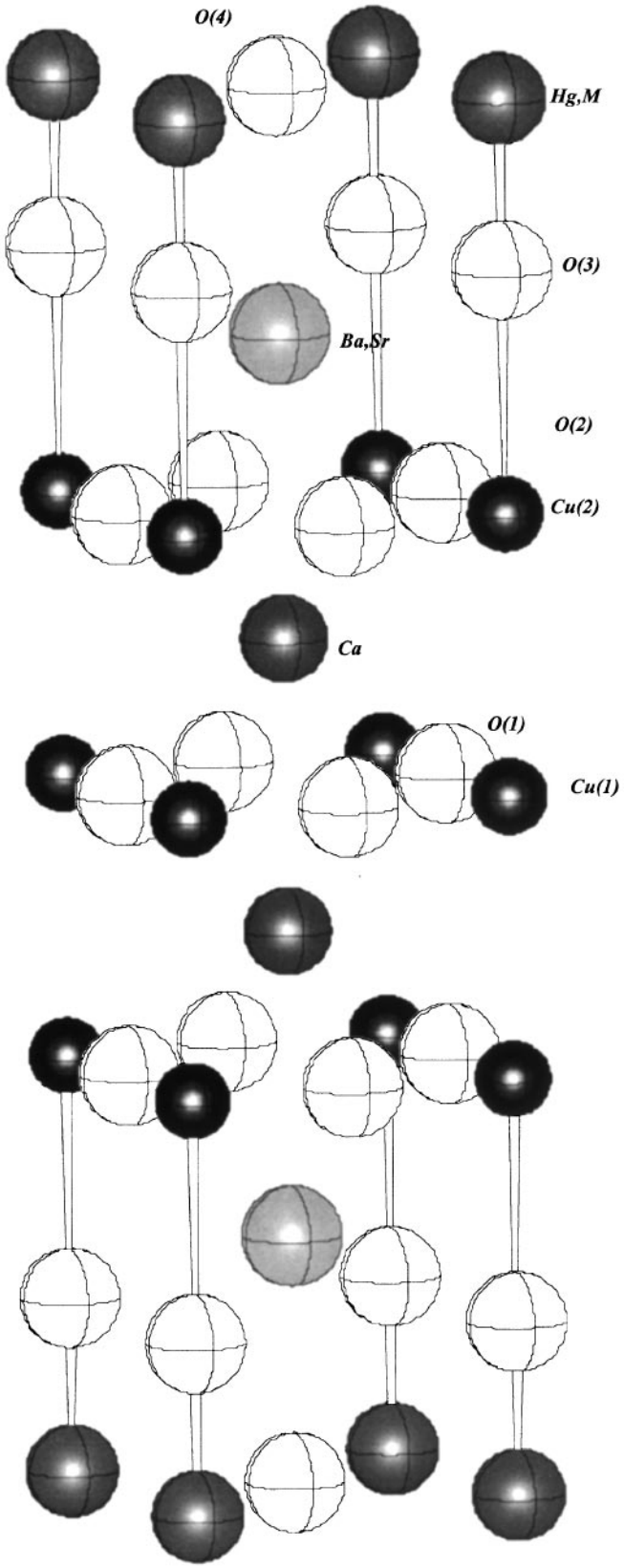

FIG. 6. Structure of the Hg-1223 system. The bonded atoms are a guide for the Hg–$O_{(3)}$–Cu and Re–$O_{(3)}$–Cu stretching modes.

Re–$O_{(3)}$ appears at higher energies. This peak assignment is in agreement with other Raman studies of the same phase and also with other low and high members of the (Hg,Re)-12($n-1$)n family (28).

The high-frequency spectrum comprises peaks at about 749, 780, 798, 807, and 862 cm^{-1}. These Raman signals are intrinsic to the Re-doped phase as has been demonstrated in Ref. (28). On the basis of the selection rules analysis, these authors attribute the peak at 749 cm^{-1} to the isotropic breathing mode caused by the Re–$(O)_6$ octahedral unit existing in the isolating block that could be acting as a pseudomolecular complex. The peaks at 780 and 798 cm^{-1} were assigned to the in-phase and out-of-phase vibrations along the c-axis of the four oxygen ions of the Re–$(O)_6$ octahedron lying on the HgO plane. Finally, the high-frequency peaks at 807 and 862 cm^{-1} were attributed to vibrations of the in-plane ions of the Re–$(O)_6$ octahedra along the x- and y-axes. Actually, the vibrations of the in-plane oxygen ions should not be Raman active because they are located in a center of inversion of the unit cell. However, those oxygen ions do not occupy the (0.5, 0.5, 0) ideal positions, but they are shifted toward the rhenium ion and strongly bounded to it (22). This fact destroys the local symmetry of the in-plane oxygen in the lattice and favors the appearance of the related modes in the Raman spectra. The authors of Ref. (28) suggested also that such phonon modes gain Raman polarizability because of the bonding of the plane oxygen to the barium ions, which are lying below them.

According to this mode assignment, we expect to see some difference in the peak frequency due to the strontium substitution in the barium site. The peaks at 780 and 798 cm^{-1} are hard to define in our spectra for $x = 0.0$, and we observe a broadening with increasing Sr substitution. The other high-frequency peaks, however, are better defined. Only the highest frequency mode at 862 cm^{-1} shows a clear decrease in frequency with increasing Sr content. We attribute these changes to the influence of the Sr ions on the vibration modes of the oxygen octahedra surrounding the rhenium ions.

In the low-frequency region, a peak of A_{1g} symmetry is observed at 98 cm^{-1} for the $x = 0.0$ sample. This peak has been assigned either directly to the Ba vibration mode along the c-axis (28, 29), or to a mixed type vibration of A_{1g} symmetry involving all the metal ions Ba, Ca, and Cu (30). The substitution of Ba by the lighter element Sr causes a shift toward higher frequencies of this mode (inset of Fig. 5). Nevertheless, other authors assign this mode to a Hg vibration (24, 31).

We are now going to explain the changes observed in the frequency of the modes related to the apical oxygens of the blocking block. It is reasonable to expect that the main decrease of the c-axis corresponds to the contraction of the blocking block as has been shown by the data taken in Re-doped samples, including complete Sr substitution (15) and Sr-free samples (22). One then expects to have some frequency variations in the Raman modes that are associated with the bonds related to this block layer (31). The frequency variation with strontium content of the modes related to the Hg–$O_{(3)}$–Cu and Re–$O_{(3)}$–Cu bonds is shown in Fig. 7. We see that both modes increase in frequency with increasing Sr content. This variation may be attributed to the change of the Re–$O_{(3)}$, Hg–$O_{(3)}$, and Cu–$O_{(3)}$ bonds induced by the strontium substitution, in the same way as shown in the Pb-doped Hg-1223 system (31). To obtain an approximate estimation of the bond length change, we use an approach similar to that applied to Y-123 and (Hg,Pb)-1223 both partially substituted by Sr (31, 32). This model assumes the following relationship between bond lengths and phonon frequency,

$$\omega_o^2 = \frac{A_{\text{Cu-O}}}{r_{\text{Cu-O}}^3} + \frac{B_{M\text{-O}}}{r_{M\text{-O}}^3},$$

where $r_{M\text{-O}}$ corresponds to Hg–O or Re–O distances. As has been previously demonstrated (31), we can assume the values of $A_{\text{Cu-O}} = 2.04 \times 10^6$ cm^{-2} $Å^3$ and $B_{\text{Hg-O}} = 1.79 \times 10^6$ cm^{-2} $Å^3$. The value of $B_{\text{Re-O}} = 2.44 \times 10^6$ cm^{-2} $Å^3$ was calculated from the bond lengths obtained from neutron measurements in Sr-free (Hg,Re)-1223 samples (22) and our Raman data.

Figures 8a, and 8b show the variation of $\Delta r_{\text{Hg-O}}$ and $\Delta r_{\text{Cu-O}}$ for the Hg–O_{ap}–Cu bond, and the variation of $\Delta r_{\text{Re-O}}$ and $\Delta r_{\text{Cu-O}}$ for the Re–$O_{(3)}$–Cu bond with respect to the Sr-free sample (M–$O_{\text{Sr},0}$–M–$O_{\text{Sr,i}}$). From these data we can observe that the decrease of the Hg–Cu and Re–Cu bonds is

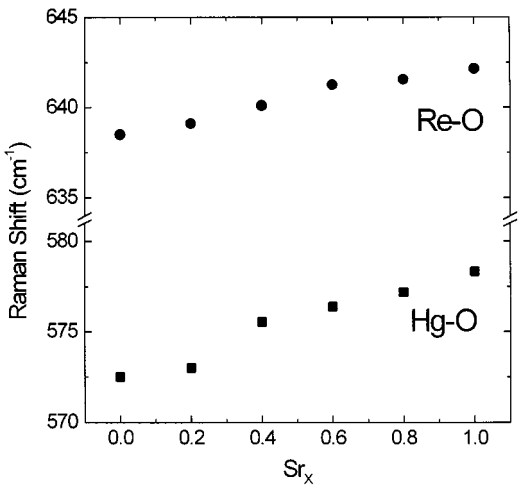

FIG. 7. Change in the Raman frequency of the apical oxygen modes in $Hg_{0.75}Re_{0.25}Ba_{2-x}Sr_xCa_2Cu_3O_y$ with Sr content.

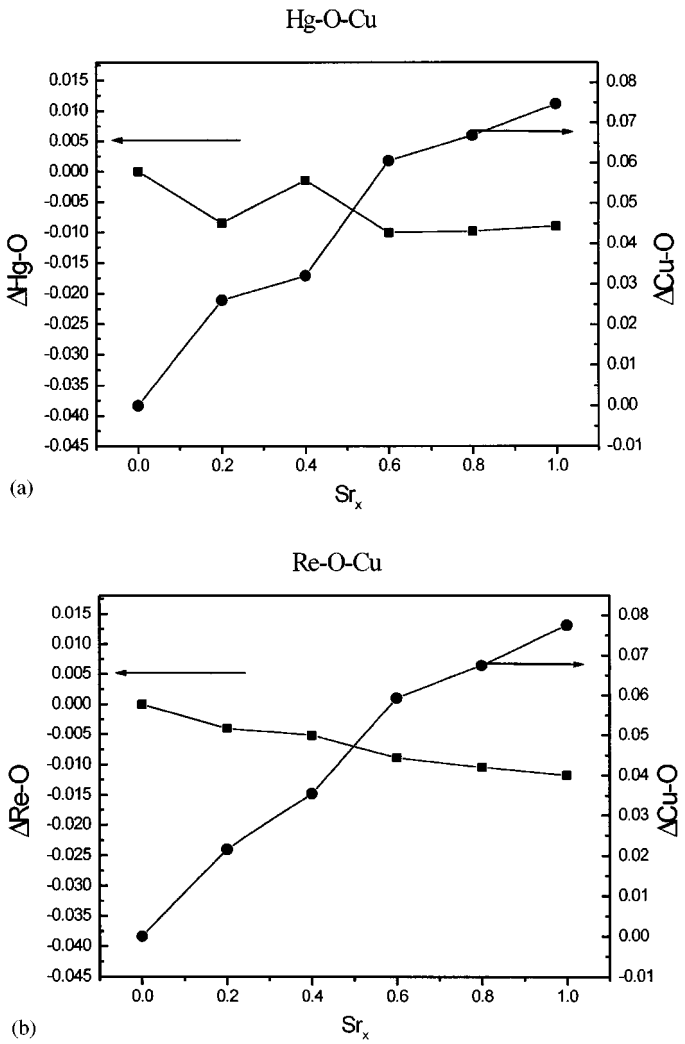

FIG. 8. Variation of r_{Hg-O} and r_{Cu-O} for the Hg–O–Cu bond (a), variation of r_{Re-O} and r_{Cu-O} for the Re–O–Cu bond (b) with respect to the Sr-free sample.

The rhenium is coordinated octahedrally with O atoms and forms much shorter M–O bond lengths with the δ oxygen ($Re–O_{(4)} = 1.86(5)$ Å (Ref. 22)) than the corresponding $Hg–O_{(4)}$ (2.725 Å (Ref. 34)). Also, the $M–O_{(3)}$ distance is slightly shorter in the rhenium-doped phase (1.92(5) Å (Ref. 22)) than the corresponding length without rhenium (1.980 Å (Ref. 35)). Thus, the rigid (Hg,Re)–$O_{(3)}$ bonds cause the $Cu–O_{(3)}$ distance to undergo the higher part of the total contraction in Hg–Cu and Re–Cu bonds. This situation contrasts with the Pb-doped (Hg,Pb)-1(Sr)223 system (31), in which the $Pb–O_{(3)}$ bond is much softer and the $Pb–O_{(3)}$ and $Cu–O_{(3)}$ bonds are compressed almost to the same extent with increasing Sr substitution.

3.3 *Superconducting Properties*

One of the most interesting parameters for practical applications in high-temperature superconductors is the irreversibility line (IL). The interest of this parameter remains in that it separates the region where the superconductor has a $j_c > 0$ from the other where $j_c = 0$. Figure 9 presents the temperature dependence of the IL for powder $Hg_{0.75}Re_{0.25}Ba_{2-x}Sr_xCa_2Cu_3O_{8+\delta}$ samples with $x = 0.0$, 0.2, 0.6, and 1.0. We defined the IL as the point where the magnetization field cool and zero field cool curves split. It is observable that the IL goes to higher values when the Sr substitution decreases. Also, we can see that the samples $x = 0.2$ and 0.6 show the same values. We can then say that the introduction of the Sr in the (Hg,Re)-1223 does not produce an increase of the IL, as was shown in Refs. (36, 37). The consequent H_{irr} vs $1 - T/T_c$ diagram indicates that the temperature dependence of all samples can be described as the power law $H_{irr}(T) \propto (1 - T/T_c)^n$ (inset Fig. 9). It is generally accepted that $n = 2$ implies 3D vortex lines, while $n = 4$ is associated with 2D vortices (38). In these samples, n moves 1.9 ($x = 1.0$) up to 2.1 ($x = 0$), which suggests that

mainly due to the compression of the $Cu–O_{(3)}$ bond in both cases, and that $Hg–O_{(3)}$ and $Re–O_{(3)}$ behave more rigidly. The rigidity of the $O_{(3)}$–Hg–$O_{(3)}$ bond is coincident with the (Hg,Pb)-1(Sr)223 system (31). Moreover, the contraction of the Hg–Cu bond due to the application of high external pressure goes in the same way (23). The $O_{(3)}$–Hg–$O_{(3)}$ bond has a structure similar to the one observed in the HgO solid compound (33). In this binary oxide one observes infinite chains composed by HgO_2 "dumb-bell" structures, which have a strong and linear bonding in the intrachain structure. This suggests that the bonds have a natural tendency to be quite rigid. On the other hand, the introduction of Sr induces also a smaller decrease in the $Re–O_{(3)}$ bond lengths. This means that the $Re–O_{(3)}$ bonds are quite rigid due to the high charge/radii ratio value (10.9) as has been mentioned before.

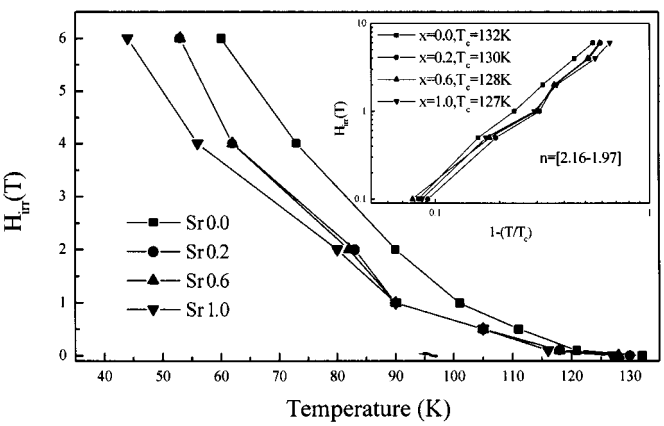

FIG. 9. Irreversibility lines of $Hg_{0.75}Re_{0.25}Ba_{2-x}Sr_xCa_2Cu_3O_y$ ($x = 0.0$, 0.2, 0.6, 1.0). Inset shows H_{irr} vs reduced temperature.

their vortex lines have a 3D behavior even at high temperatures and high fields.

In a first approach, to explain the decreasing IL values with increasing strontium substitution, we would need a slight underdoping of the samples by Sr substitution. The decrease of T_c (values given in Fig. 9) with the IL behavior could be a sign of this supposition. Otherwise, if our samples were overdoped we should see an increase of the IL values (37). Nevertheless, other works (10, 40) show superconductivity at 109 K for a (Hg,Re)-1223 system with a total strontium substitution with a sealed-tube technique and T_c rises to 114 K after annealing in a reducing atmosphere (10% H_2/90% N_2) (10). In the same way, for a sample prepared under high pressure T_c goes up to 120 K after a vacuum annealing (40). Therefore, certainly these samples are strongly overdoped.

Measurements under pressure can be an excellent tool to determine the degree of doping of a cuprate material (41). A typical example is the case of cuprocarbonate cuprates. As-prepared samples show a higher T_c for the four-layer material than for the three-layer one, but pressure measurements showed that the three-layer samples were overdoped (42). Desoxygenation experiments done later confirmed this conclusion (43). Thus, in order to check if our samples are in the overdoped or underdoped regime, resistivity measurements under high pressure are performed.

In Fig. 10 we show the evolution of T_c with the physical pressure applied on a ceramic of $Hg_{0.75}Re_{0.25}Ba_{2-x}Sr_xCa_2Cu_3O_{8+\delta}$ for $x = 0.0$ and $x = 1.0$. The T_c is measured by the resistivity of a small piece of the ceramic (millimetric size) mounted on the pressure cell (41). The peak of the resistivity derivative respect to the temperature determines the T_c. The T_c rises almost linearly up to 9.5 GPa with a rate (dT_c(K)/dP(GPa)) of 0.9 K/GPa for $x = 0.0$ and the same for $x = 1.0$. These values are smaller than the ones measured in Sr-free samples without rhenium and optimally doped (1.7 K/GPa) (44). After 9.5 GPa we observe a decrease of this rate in both cases and T_c begins to saturate. In the first linear regime, the rise of T_c is attributed to the intrinsic effect. This results from a geometry change of the CuO_2 planes towards a more favorable geometry for increasing T_c. On the other hand, charge transfer between the reservoir and the superconducting block due to volume reduction controls the parabolic term of the curve (44).

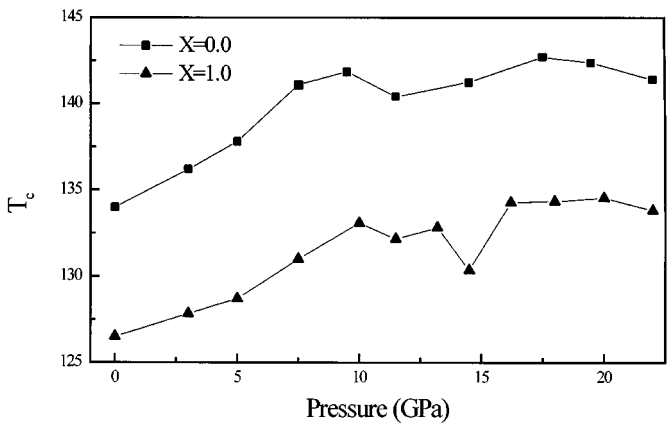

FIG. 10. T_c values obtained from resistivity measurements under high external pressure in $Hg_{0.75}Re_{0.25}Ba_{2-x}Sr_xCa_2Cu_3O_y$ ($x = 0.0$ and 1.0).

In mercury cuprates such as $HgBa_2Ca_2Cu_3O_{8+\delta}$, even overdoped samples show an increase of T_c under pressure because intrinsic effects are supposed to be more efficient than charge transfer (45). In the overdoped sample ($T_c = 127$ K) a rate of 0.7 K/GPa is described (45). Therefore, comparing this rate with the one obtained for our samples, we can see that they are closer to the overdoped samples than to the optimally doped situation. Another interesting characteristic to observe is that the saturation of the T_c rise is not seen in nondoped Hg-1223, in contrast to our samples, behavior. They also show a clear decrease of T_c after $\sim$20 GPa, as in the case of overdoped samples (45). In this last region of pressure it is supposed that the charge transfer becomes more important, and the samples reach a typical overdoped regime. In agreement with this reasoning, the maximum T_c values obtained are 143 K and 134 K for the (Hg,Re)-1223 Sr-free system and for the 50% Sr substitution, respectively. These values are lower than the ones measured in the (Hg)-1223 system, but they are close to those of the overdoped sample ($T_c = 138$ K) (45).

Therefore, from this analysis we can say that these samples seem to be in the overdoped regime. Nevertheless, the overdoped degree of our samples is very low (taking into account the T_c value at ambient pressure), compared to the data reported in Refs. (10,40). This could mean that the overdoping is obtained under the thermal treatment conditions applied in the synthesis process. In a previous work it was demonstrated that the final oxygen content of the (Hg,Re)-1223 as-prepared superconducting samples (39, 46) can be defined during the precursor synthesis.

Another interesting feature is observed in this experiment. At saturation T_c shows in fact two relative maxima in both cases. This phenomenon may be explained if we take into account different doping for nonequivalent cuprate planes (47), already discussed in the analysis of screening lengths by NMR in Tl compounds (48, 49). On the other hand, a similar evolution, but in the overdoped regime (T_c decreasing with applied pressure), has been seen in T1-2223 and T1-2234 systems (50). This issue is still under study.

Comparing the data of resistivity under high pressure and the IL, one can conclude that an overdoped regime with a reduction of the blocking block due to the Sr substitution does not produce an increase of the IL. In general, the excess of oxygen in the $M_mA_2Q_{n-1}Cu_nO_{m+2+2n\pm\delta}$ cuprate system was believed to produce (51) (i) a thinner AO–$M_mO_{m\pm\delta}$–AO

blocking block, (ii) an increase in the hole doping in the $Q_{n-1}Cu_nO_{2n}$ superconducting block, and (iii) some of the doped holes also in the blocking block. It is demonstrated for the $Cu(Ba_{0.8}Sr_{0.2})_2(Yb_{1-x}Ca_x)Cu_2O_{7-\delta}$ system that the enhancement of the IL is mainly due to points (ii) and (iii) (52). On the other hand, the increase of the oxygen content with a reduction of the blocking block produces a reduction of the H_{irr} in the $Bi_2Sr_2(Ca_{1-x}Y_x)Cu_2O_{8+\delta}$ system (53). With these data, the authors remark that in the multilayered copper oxide structures the more homogeneous hole distribution along the piling direction of different blocks is the main parameter that controls the IL.

The value of the hole concentration, using the BVS (bond valence sum) method (51), was calculated from the valances of the in-plane copper and oxygen atoms, and it was shown that the contributions from the in-plane Cu–O bonds are counteracted and only the bonds from Cu to the apical oxygen ($O_{(3)}$) and from in-plane O to the Q (Ca) and A (Ba,Sr) cations have net effects on the hole concentration (54). Related to the three hole-doping routes mentioned before, it could be written now in the following form: (i) reduction of the $Cu–O_{(3)}$ bond and (ii) lengthening of the effective distance of the in-plane oxygen to the A (Ba,Sr) atom or (iii) to the Q (Ca) atom (54).

Applying this reasoning in the (Hg,Re)-1(Sr)223 samples we can understand the decrease of the IL. The reduction of the $Cu–O_{(3)}$ bond is a parameter that is satisfied as was discussed from the Raman spectrum data obtained. Furthermore, if we take the neutron data analysis reported in Ref. (15, 22), the $Ca–O_{(2)}$ and $Ba–O_{(2)}$ distances in the Re-doped and Sr-free samples are 2.451(3) and 2.777(4) Å, respectively (22). While for a total Sr-substituted sample they are 2.471(4) Å for the $Ca–O_{(2)}$ bond and 2.641(4) Å for the $Sr–O_{(2)}$ (15). A very important reduction of the A–O bond is observed due to the strontium that also produces a less important elongation of the Ca–O bond. This fact with the high valance of the rhenium may be the cause of a nonhomogeneous hole-doping in the Sr substitution and reduces the IL in contrast to the Sr-free samples.

4. CONCLUSION

The study of the structural and superconducting properties of $Hg_{0.75}Re_{0.25}Ba_{2-x}Sr_xCa_2Cu_3O_{8+\delta}$ compounds provides new information about the influence of the Sr substitution in the mercury system doped with rhenium. The efficiency of c-axis reduction caused by the Sr substitution depends on the environment in the (Hg,N)–O layer. Therefore, in a rhenium-doped system the solubility of the Sr is lower than for other less acidic cations, such as Pb^{4+}. This fact is understood by taking into account the rigidity found for the $Re–O_{(3)}$ bond by micro-Raman analysis. We have found that the higher IL values correspond to Sr-free samples and they decrease with increasing Sr substitution. Moreover, the IL measurements show that the vortex lines have a 3D behavior for all the samples with n values in the 2.1–1.9 range. Finally, it is shown that the as-prepared samples display an overdoped regime as is observable by the resistivity measurements under high pressure.

ACKNOWLEDGMENTS

A.S. thanks the chemical department of CNRS for financially supporting his stay in Grenoble. We are pleased to thank DIOPMA S.L. (Barcelona) for their kind supply of high-purity oxides and carbonates.

REFERENCES

1. A. Schilling, M. Cantoni, J. D. Guo, and H. R. Ott, *Nature* **363,** 56 (1993).
2. C. W. Chu, L. Gao, F. Chen, Z. J. Huang, R. L. Meng, and Y. Y. Xue, *Nature* **365,** 323 (1993).
3. M. Nùñez-Regueiro, J.-L. Tholance, E. V. Antipov, J.-J. Capponi, and M. Marezio, *Science* **262,** 97 (1993).
4. M. Núñez-Regueiro and C. Acha, (A. Narlikar, Ed.), Vol. 24, Nova Science Publisher, New York, 1997.
5. Z. H. He, Q. M. Lin, L. Gao, Y. Y. Sun, Y. Y. Xue, and C. W. Chu, *Physica C* **241,** 211 (1995).
6. A. Sin, P. Odier, M. Núñez-Regueiro, M. T. D. Orlando, and A. G. Cunha, *in* "Applied Superconductivity'99, Proceedings of EUCAS 1999, The European Conference on Applied Superconductivity" (X. Obradors, F. Sandiumenge, and J. Fontcuberta, Eds.), Institute of Physics Conference Series, No. 167, p. 283, 2000.
7. M. Marezio and F. Licci, *Physica C* **282–287,** 53 (1997).
8. S. Lee, T. Akao, H. Suematsu, H. Yamauchi, N. P. Kiryakov, D. A. Emelyanov, and M. S. Kuznetsov, *Appl. Phys. Lett.* **73,** 3586 (1998).
9. M. A. Subramanian and M. H. Whangbo, *J. Solid State Chem.* **109,** 410 (1994).
10. N. C. Hyatt, G. B. Peacock, I. Gameson, K. L. Moran, M. Slaski, M. O. Jones, A. J. Ellis, Y. E. Gold, R. Dupree, and P. P. Edwards, *Int. J. Inorg. Mater.* **1,** 87 (1999).
11. A. Sin, P. Odier, and M. Núñez-Regueiro, *Physica C* **330,** 9 (2000).
12. A. Sin, L. Fàbrega, M. T. D. Orlando, A. G. Cunha, S. Piñol, E. Bagio-Saitovich, and X. Obradors, *Physica C* **328,** 80 (1999).
13. A. Sin and P. Odier, *Adv. Mater.* **12,** 649 (2000).
14. A. Sin, A. G. Cunha, A. Calleja, M. T. D. Orlando, F. G. Emmerich, E. Baggio-Saitovich, S. Piñol, J. M. Chimenos, and X. Obradors, *Physica C* **306,** 34 (1998).
15. O. Chmaissem, J. D. Jorgensen, K. Yamaura, Z. Hiroi, M. Takano, J. Shimoyama, and K. Kishio, *Phys. Rev. B* **53,** 14647 (1996).
16. K. Kishio, J. Shimoyama, A. Yoshikawa, K. Kitazawa, O. Chmaissem, and J. D. Jorgensen, *J. Low Temp. Phys.* **105,** 1359 (1996).
17. K. Yamura, J. Shimoyama, S. Hahakura, Z. Hiroi, M. Takano, and K. Kishio, *Physica C* **246,** 351 (1995).
18. E. Kandyel, S. Adachi, X. J. Wu, and S. Tajima, *Supercond. Sci. Technol.* **12,** 1168 (1999).
19. Z. H. He, Q. M. Lin, L. Gao, Y. Y. Sun, Y. Y. Xue, and C. W. Chu, *Physica C* **241,** 211 (1995).
20. S. Lee, M. Kuznetzov, N. Kyriakov, D. Emelyanov, and Y. Tretyakov, *Physica C* **290,** 275 (1997).
21. J. L. Wagner, B. A. Hunter, D. H. Hinks, and J. D. Jorgensen, *Phys. Rev. B* **51,** 15407 (1995).
22. O. Chmaissem, P. Guptasarma, U. Welp, D. G. Hinks, and J. D. Jorgensen, *Physica C* **292,** 305 (1997).

23. M. Marezio and J. Chenevas, *J. Solid State Chem.* **121,** 24 (1996).
24. X. Zhou, M. Cardona, C. W. Chu, Q. M. Lin, S. M. Loureiro, and M. Marezio, *Physica C* **270,** 193 (1996).
25. I. S. Yang, H. G. Lee, N. H. Hur, and J. Yu, *Phys. Rev. B* **52,** 15078 (1995).
26. Y. Zhou, M. Cardona, C. W. Chu, Q. M. Lin, S. M. Loureiro, and M. Marezio, *Phys. Rev. B* **54,** 6137 (1996).
27. M. T. D. Orlando, A. Sin, F. Alsina, A. G. Cunha, N. Mestres, A. Calleja, S. Piñol, F. G. Emmerich, L. G. Martinez, M. Segarra, X. Obradors, and E. Baggio-Saitovitch, *Physica C* **328,** 257 (1999).
28. N. Poulakis, D. Lampakis, E. Liarokapis, A.Yoshikawa, J. Shimoyama, K. Kishio, G. B. Peacock, J. P. Hodges, I. G. Gameson, P. P. Edwards, and C. Panagopoulos, *Phys. Rev. B* **60,** 3224 (1999).
29. A. Sacuto, A. Leblon, D. Colson, A. Bertinotti, J.-F. Marucco, and V. Viallet, *Physica C* **259,** 209 (1996).
30. X. Zhou, M. Cardona, C. Colson, and V. Viallet, *Phys. Rev. B* **55,** 12770 (1997).
31. S. Lee, N. P. Kiryakov, D. A. Emelyanov, M. S. Kuznetsov, Y. D. Tretyakov, V. V. Petrykin, M. Kakihana, H. Yamauchi, Y. Zhuo, M.-S. Kim, and S.-I. Lee, *Physica C* **305,** 57 (1998).
32. M. Kakihana, S. G. Eriksson, L. Börjsson, L. G. Johansson, C. Ström, and M. Käll, *Phys. Rev. B* **47,** 5359 (1993).
33. N. C. Hyatt, J. P. Hodges, I. Gameson, S. Hull, and P. P. Edwards, *J. Solid State Chem.* **148,** 119 (1999).
34. J. Karpinski, H. Schwer, R. Molinski, G. I. Meijer, E. Kopnin, M. Angst, S. Büchi, J. Hofer, V. Alyishin, R. Puzniak, and A. Wisniewski, *in* "High-Temperature Superconductors and Novel Inorganic Materials" (G. Van Tendeloo, E. V. Antipov, and S. N. Putilin, Eds.), pp. 21–26. Kluwer Academic, Dordrecht, 1998.
35. G. B. Peacock, Z. Zhou, and P. P. Edwards, "Studies of High Temperature Superconductors" Vol. 25, pp. 185–227. Nova Science Publishers, New York, 1998.
36. K. Kishio, J. Shimoyama, A. Yoshikawa, K. Kitazawa, O. Chmaissem, and J. D. Jorgensen, *J. Low Temp. Phys.* **105,** 1359 (1996).
37. J. Shimoyama, *Supercond. Sci. Technol.* **13,** 43 (2000).
38. G. Blatter, M. V. Fiefel'man, V. B. Geshkenbein, A. I. Larkin, and V. M. Vinokur, *Rev. Mod. Phys.* **66,** 1125 (1994).
39. A. Sin, P. Odier, A. G. Cunha, M. T. D. Orlando, S. Piñol, E. Baggio-Saitovich, and X. Obradors, *Supercond. Sci. Technol.* **12,** 1175 (1999).
40. K. Yamaura, J. Shimoyama, S. Hahakura, Z. Hiroi, M. Takano, and K. Kishio, *Physica C* **246,** 351(1995).
41. M. Núñez-Regueiro and C. Acha, "Studies of High Temperature Superconductors" (A. Narlikar, Ed.), Vol. 24. Nova Science Publisher, New York, 1997.
42. M. Núñez-Regueiro, M. Jaime, M. A. Alario-Franco, J.-J. Capponi, C. Chaillout, J.-L. Tholence, A. Sulpice, and P. Lejay, *Physica C* **235–240,** 2093 (1994).
43. C. Chaillout, S. Le Floch, E. Gautier, P. Bordet, C. Acha, Y. Feng, A. Sulpice, J. L.Tholence, and M. Marezio, *Physica C* **266,** 215 (1996).
44. M. Núñez-Regueiro, J.-L. Tholance, E. V. Antipov, J.-J. Capponi, and M. Mareizo, *Science* **262,** 97 (1993).
45. C. Acha, M. Núñez-Regueiro, S. Le Floch, P. Bordet, J.-J. Capponi, C. Chaillout, and J.-L. Tholence, *Phys. Rev. B* **57,** 5630 (1998).
46. A. Sin, A. G. Cunha, A. Calleja, M. T. D. Orlando, F. G. Emmerich, E. Baggio-Saitovich, M. Segarra, S. Piñol, and X. Obradors, *Supercond. Sci. Technol.* **12,** 120 (1999).
47. M. Di Stasio, K. A. Müller, and L. Pietronero, *Phys. Rev. Lett.* **64,** 2827 (1990).
48. A. Trokiner, L. Noc, J. Schneck, A. M. Pougnet, R. Mellet, J. Primot, H. Savary, Y. M. Gao, and S. Aubry, *Phys. Rev. B* **44,** 2426 (1991).
49. Y. V. Piskunov, K. N. Mikhalev, Y. I. Zdhanov, A. P. Gerashenko, S. V. Verkoskii, K. A. Okulova, E. Y. Medvedev, A. Y. Yakubovskii, L. D. Shustov, P. V. Bellot, and A. Trokiner, *Physica C* **300,** 225 (1998).
50. D. Tristan Jover, R. J. Wijngaarden, R. Griesen, E. M. Haines, J. L. Tallon, and R. S. Liu, *Phys. Rev. B* **45,** 3172 (1989).
51. M. Karppinen and H. Yamauchi, *Philos. Mag. B* **79,** 343 (1999).
52. T. Nakane, F. Fujinami, M. Karppinen, and H. Yamauchi, *Supercond. Sci. Technol.* **12,** 242 (1999).
53. M. Karppinen and H. Yamauchi, *Mater. Sci. Eng.* **26,** 51 (1999).
54. H. Yamauchi and M. Karppinen, *J. Low Temp. Phys.* **117,** 813 (1999).